

# A HIGHLY COLLIMATED BIPOLAR OUTFLOW IN A PROTOPLANETARY NEBULA: *HST* IMAGING OF HEN 401<sup>1</sup>

Raghvendra Sahai<sup>2</sup>, V. Bujarrabal<sup>3</sup>, A. Zijlstra<sup>4</sup>

Received \_\_\_\_\_; accepted \_\_\_\_\_

---

<sup>1</sup>Based on observations with the NASA/ESA *Hubble Space Telescope*, obtained at the Space Telescope Science Institute, which is operated by AURA Inc., under NASA contract 5-26555

<sup>2</sup>Jet Propulsion Laboratory, MS 183-900, California Institute of Technology, Pasadena, CA 91109

<sup>3</sup>Observatorio Astronómico Nacional, Ap. 1143, 28800 Alcala de Henares, Spain

<sup>4</sup>UMIST, Department of Physics, PO Box 88, Manchester M60 1QD, UK

## ABSTRACT

We have obtained high-resolution wide- and narrow-band images of the bipolar protoplanetary nebula Hen 401 with the Wide-Field & Planetary Camera 2 onboard the *HST*. Two very long ( $14''.5$ ), cylindrical-shaped bipolar outflow lobes are seen in reflected light, each with a length/width ratio of  $\approx 7$ , probably the largest seen in a protoplanetary nebula so far. The lobes are limb-brightened indicating that they are optically-thin to scattering. The central star, resolved for the first time from the surrounding nebulosity, is girdled by an equatorial torus and a bipolar skirt-like structure, both of which are co-axial with the lobes. A faint halo around the lobes marks the presence of a surrounding AGB envelope. We find  $H\alpha$  emission from photoionized gas in the vicinity of the central star, and tentatively detect two small shock-emitting blobs located along the nebular axis about  $\pm 6''.2$  from the central star. Comparison of the lobe morphology with theoretical models indicates that the highly-collimated lobes of Hen 401 result from the momentum-driven shock interaction of a high-velocity bipolar jet with the circumstellar envelope of the progenitor AGB star.

*Subject headings:* planetary nebulae, stars: AGB and post-AGB, stars: mass-loss, circumstellar matter

## 1. Introduction

Most planetary nebulae (PNs) deviate from spherical symmetry (e.g. Schwarz, Corradi, & Melnick 1992, Aaquist & Kwok 1991), a result dramatically supported by recent  $H\alpha$  imaging of young PNs (Sahai & Trauger 1998, hereafter ST98). In the generalised interacting stellar winds (“GISW”) model, a variety of axisymmetric PN shapes are obtained by the interaction of a very fast central star wind with the progenitor AGB circumstellar envelope (CSE) (Kwok 1982), when the latter is denser near the equator than the poles (Balick 1987). However, the presence of jets/collimated outflows, FLIERs (Balick et al. 1998), and multipolar and point-symmetric structures in PNs (ST98) and protoplanetary nebulae (PPNs) (Sahai et al. 1999a), do not fit into the GISW scenario, strongly suggesting that additional shaping mechanisms are required. ST98 have proposed that collimated fast outflows operating during the very late AGB or PPN phase are the primary agents in the formation of aspherical PNs. Because most PPNs are small in angular size (e.g. Hrivnak et al. 1999), we are carrying out high angular-resolution imaging of these objects with *HST* (Bujarrabal et al. 1998; Sahai et al. 1998ab,1999ab) in order to characterise their structure and better constrain PN formation theories.

Hen 401 is a bipolar ( $\sim 25'' \times 10''$ ) reflection nebula surrounding a reddened B1 (post-AGB) star [Sanduleak & Stephenson 1973, Allen (1978) & Bujarrabal & Bachiller (1991) (hereafter BB91)]. The distance to Hen401 is not well-known; BB91 estimate a value of 3 kpc (which we have adopted). BB91 find CO line emission at 2.6 & 1.3 mm, implying the presence of a dense extended molecular envelope expanding at  $15 \text{ km s}^{-1}$ . In this Letter, we report *HST* images of Hen 401: the extreme aspherical morphology uncovered provides

## 2. Observations

The observations were obtained on 1997 Dec 6, with the Planetary Camera of the Wide Field & Planetary Camera 2 (800x800 pixels with a plate scale of  $0''.0456/\text{pixel}$ ) onboard *HST*, through the wideband F606W filter ( $\langle \lambda \rangle = 593.5 \text{ nm}$ ,  $\delta\lambda = 149.7 \text{ nm}$ ), and narrow-band emission-line filters ( $\text{H}\alpha$ , F656N and  $[\text{SII}]$ , F673N). A total of 8 pipeline-calibrated exposures were retrieved (F606W -  $2 \times 200 \text{ s}$  &  $2 \times 400 \text{ s}$ ; F656N -  $2 \times 200 \text{ s}$ ; and F673N -  $2 \times 400 \text{ s}$ ), and were corrected for saturation effects and cosmic-ray hits.

## 3. Results

### 3.1. Optical Morphology

The F606W PC image of Hen 401 is displayed in Fig. 1(a); Fig. 1(b) shows the same image processed in order to emphasize sharp structures. The images show highly collimated, cylindrical-shaped bipolar lobes, with tattered ends. Each lobe is very long, with a length/width ratio of  $\approx 7$ , probably the largest seen in any PPN so far. In Fig. 1b, intricate filamentary structures can be seen in the lobe region. The central star, resolved for the first time from the surrounding nebulosity, appears to lie at the center of a bipolar “skirt” structure co-axial with the lobes. Separating the bipolar lobes, and girdling the star, is an equatorial band (also co-axial with the lobes), which could be the “disk” inferred from ground-based polarisation imaging by Scarrott & Scarrott (1995). The west lobe is brighter than the east one by 0.95 magnitudes. A faint elliptical halo surrounds the central regions of the lobes. The total nebular flux is about 42 mJy, with roughly 2.5% arising in the halo. The central star coordinates (J2000) measured from our *HST* data are  $\alpha = 10^{\text{h}} 19^{\text{m}} 32^{\text{s}}.52$ ,  $\delta = -60^{\circ} 13' 29''.3$ .

### 3.2. H $\alpha$ Emission

The F656N and F673N images of Hen401 are almost identical to the scattered-light F606W image, indicating that we are mostly seeing scattered light in the narrow-line filters also. However, in the F656N image, the count rate is typically (7.5–10) times larger than the contribution estimated for the scattered continuum of a reddened (with  $E_{B-V}=2$ ) B1 star, using the observed counts in the F606W image. This implies that the F656N image is dominated by scattered H $\alpha$  emission from the vicinity of the central star. The counts in the F673N image are roughly consistent with those expected from the scattered continuum. Thus, there is no *strong* optical emission-line flux which arises within the nebular lobes, consistent with the low stellar  $T_{eff}$  (22000K).

In order to search for ionized emission, we have constructed F656N/F606W and F673N/F606W ratio images (Fig. 1c,d). A X-shaped structure, corresponding to the inner regions of the skirt, stands out prominently in these images, implying large variations in the two ratios in the central star vicinity. Both ratios will simultaneously increase in regions of increasing nebular extinction because of the lower extinction in the wavelength ranges covered by the narrow F656N and F673N filters, compared to the broad F606W filter. However, this effect cannot explain the enhanced F656N/F606W ratio in the central star vicinity, because the F656N/F606W and F673N/F606W ratio images appear *complementary* to each other – the X-shaped structure is bright in the former and dark in the latter. We therefore conclude that the inner regions of the skirt (X-shaped region in Fig. 1c) show H $\alpha$  emission. The complementarity of the two ratio images is due to the inclusion of the H $\alpha$  emission line in the F606W filter, which enhances the counts in the F606W image and diminishes the F673N/F606W ratio in regions of relatively intense H $\alpha$  emission.

The central star and its immediate surroundings show the largest values of the F656N/F606W ratio, and support our earlier conclusion that most of the H $\alpha$  emission

arises very close to the central star. This emission is probably due to recombinations in gas photoionized by the stellar continuum and not by shocks: (i) The bulk of the  $H\alpha$  emitting gas lies near the star ( $\lesssim 2 \times 10^{16}$  cm) and its spatial distribution peaks at the stellar position, where maximum photoionization is expected. In other similar objects showing collisionally excited atomic lines (e.g. He3-1475: Borkowski, Blondin, & Harrington 1997, M1-92: Bujarrabal et al. 1998), the emitting gas is found in regions significantly more distant ( $\gtrsim 10^{17}$  cm) from the star along the symmetry axis. (ii) The lack of detectable [SII] emission, and the weak optical [NII], [OI] and [SII] line emission measured by Allen (1978), is in conflict with models (e.g. Hartigan, Raymond, & Hartmann 1987) and observations of shock emission (see i), which show that these lines should be a factor  $\gtrsim 1/3$  as strong as  $H\alpha$ . (iii) The ionizing photons emitted by a B1 star are sufficient to explain the  $H\alpha$  excess detected in our observations. The Zanstra formulae for a nebula photoionized by a B1 star (e.g. Pottasch 1984), predicts a ratio  $H\beta$  (total flux) / visible continuum (flux per wavelength unit)  $\sim 50 \text{ \AA}$ . Given the expected  $H\alpha/H\beta$  line flux ratio ( $\sim 2.9$ ) and the F656N filter width (22  $\text{\AA}$ ), the  $H\alpha$  contribution within our F656N filter should be  $\sim 6.5$  times larger than the continuum, in agreement with our observations.

Most of the extended lobe regions show relatively low and uniform line ratios. However, two blobs of size  $\sim 0''.6$  with higher line ratios are seen along the nebular axis about  $\pm 6''.2$  ( $2.8 \times 10^{17}$  cm) from the central star - we regard their detection to be tentative because of the relatively poor  $[(3-5)\sigma]$  signal-to-noise ratio in this region. Since the extinction in these regions is expected to be low, the line ratios are elevated because of line emission and not because of large and variable extinction. In contrast to the skirt region, *both* line ratios are high in the blobs, indicating that the [S II]-to- $H\alpha$  ratio is significantly higher in the latter (to counteract the diminishing affect of the inclusion of  $H\alpha$  emission in the F606W passband on the F673N/F606W ratio). In light of arguments (i) and (ii) above, we conclude that the blob emission is probably due to shock-excitation.

### 3.3. The Structure of Hen 401

The extended lobes are limb-brightened, indicating that they are optically-thin to scattering, and probably best represented by cylinders with dense walls and a relatively tenuous interior. Quantitative modelling to derive the wall-thickness and wall-to-interior density contrast is complicated by significant patchiness in the lobe surface brightness profiles (see Fig. 1b), and will not be attempted here. The skirt structure appears to have an hourglass shape. The equatorial band probably demarcates a torus, with an outer radius of  $1''.4$ , girdling the central star. On the west side, the inner side of the skirt is bright and continues unbroken to the star, whereas on the east, it appears fainter and is detached from the latter, presumably as a result of obscuration by the equatorial torus, suggesting that the western half of the nebula is tilted towards us. This orientation is confirmed by velocity-resolved observations of  $2.1 \mu\text{m}$   $\text{H}_2$  line emission from Hen 401 (Sahai et al. 1999c) showing blue-shifted (red-shifted) emission from the west lobe (east lobe). The maximum velocity separation between the blue- and red-shifted emission is  $\sim 60 \text{ km s}^{-1}/\sin i$ , where  $i$  is the inclination angle of the nebular symmetry axis with the line-of-sight ( $los$ ). Considering the relatively large linear extent of the lobes which are seen in projection,  $i$  is likely to be small. The faint elliptical halo is probably due to material in the relatively undisturbed progenitor AGB CSE illuminated by scattered light from the bright lobes.

Each lobe has a width of  $(2.1\text{-}2.4)''[(9.4\text{-}11)\times 10^{16} \text{ cm}]$  and a length (measured to the outer edge of the tattered lobe ends) of  $\approx 14''.5 (6.5\times 10^{17} \text{ cm})$ . We estimate a  $0.6 \mu\text{m}$  stellar flux of  $\sim (0.16\text{-}0.24) \text{ mJy}$  from our F606W image. The intrinsic stellar flux, derived from the bolometric flux (determined from ground-based and IRAS photometry to be  $1.3 \times 10^{-8} \text{ ergs s}^{-1}\text{cm}^{-2}$ ) with  $T_{eff}=22000 \text{ K}$ , is  $0.28 \text{ Jy}$ . Hence, the extinction optical depth towards the star along the  $los$  (presumably due to the equatorial torus) is  $\sim 6.5\text{-}7$ , larger than expected from the  $A_v \approx 3 - 4$  estimated by BB91 from the ground-based optical spectrum.

We later (§5) present a qualitative model for producing the lobes. The presence of the skirt and equatorial torus in Hen 401 remains unexplained, and with the discovery of similarly geometrically distinct inner structures in young PNs (Sahai et al. 1999d, ST98), adds to a deepening mystery about the nature and origin of such structures.

#### 4. The Progenitor AGB Star: Nebular Mass, Mass-Loss Rate & Luminosity

We now constrain the mass loss from the progenitor AGB star of Hen 401 by fitting its color-corrected IRAS far-infrared fluxes (from BB91), using a multi-component dust emission model (Sahai et al. 1991). A dust emissivity of  $150 \text{ cm}^2\text{g}^{-1}$  at  $60 \mu\text{m}$  (Jura 1986), with a  $\lambda^{-p}$  power-law variation is assumed. We require at least two different temperature dust components, with temperatures of 73(81) and 500(536) K for  $p=1.5(1)$ , to fit the data. The corresponding masses are  $3.6(2.4)\times 10^{-3}$  and  $9(4)\times 10^{-7} M_{\odot}$  (and the bolometric flux and luminosity are  $1.3(1.2) \times 10^{-8} \text{ ergs s}^{-1}\text{cm}^{-2}$  &  $3.6(3.5)\times 10^3 L_{\odot}$ ). Thus the total CSE mass,  $M_{env}$ , is about  $(0.5-0.7) M_{\odot}$  assuming a typical gas-to-dust ratio of 200 for AGB CSEs. The characteristic radius of the far-infrared dust emitting region,  $r_d$ , is unknown. If the dust is heated by starlight, then  $r_d = [\frac{L_{\star}T_{\star}^p}{16\pi\sigma}]^{1/2}T_d^{-(2+p/2)}$  (Herman, Burger & Penninx 1986), and we find that  $T_d=73(81)$  K at  $r_d = 9.4(1.7) \times 10^{17} \text{ cm}$  for  $T_{\star}=22000$  K and  $p=1.5(1)$ . Thus, from the dust ejection time-scale,  $t_{exp} \sim (1.8 - 0.33) \times 10^4 \text{ yrs}$ , derived using an expansion velocity of  $V_{exp}=15 \text{ km s}^{-1}$ , we find a progenitor AGB mass-loss rate of  $\dot{M}=M_{env} / t_{exp} \sim (0.4 - 1.4)\times 10^{-4}(V_{exp}/17 \text{ km s}^{-1}) M_{\odot} \text{ yr}^{-1}$ . Our result is consistent with BB91's estimate  $\dot{M} \approx 5 \times 10^{-5} M_{\odot} \text{ yr}^{-1}$  based on CO observations. The following proportionalities apply:  $M_{env} \propto D^2$  and  $\dot{M} \propto D$ , where  $D$  is the distance to Hen401. Thus the AGB CSE mass and mass-loss rate in Hen401 are relatively high and comparable to those found for other PPNs such as M1-92 (Bujarrabal, Alcolea, & Neri 1998), Roberts 22 (Sahai et al. 1999a) and CRL2688 (Truong-Bach et al. 1990).

## 5. Discussion

In the popular GISW model, the shapes of PNs depend on the equatorial-to-polar density contrast, varying from elliptical shapes (obtained for a low contrast factor) to “butterfly” shapes (obtained for a high contrast factor). In spite of considerable sophistication in the input physics (Mellema 1995 and references therein), none of the existing GISW simulations to-date have produced such long and well collimated outflow lobes as seen in Hen 401. Other post-AGB objects exist with significantly collimated lobes such as He3-1475 (Bobrowsky et al. 1995), CRL2688 (Sahai et al. 1998b), M1-92 (Bujarrabal et al. 1998), M2-9 (Schwarz et al. 1997), and IC4406 (Sahai et al. 1991). In contrast to the GISW model, simulations of YSO jets expanding within an ambient molecular cloud produce elongated structures (e.g. Raga et al 1995, Masson & Chernin 1993: hereafter MC93) which resemble the lobes in Hen 401. For their analytical model of a momentum-conserving  $300 \text{ km s}^{-1}$  jet expanding in an  $r^{-1}$  density ambient cloud, MC93 note that the resulting lobes are cylindrical as opposed to being wider near the star where the swept-up shell has had a longer time to expand, because the ambient density law gives the highest density near the star, impeding the sideways shell-expansion. Since AGB CSEs typically follow  $r^{-2}$  density laws, they are potentially capable of producing cylindrical lobes. The tattered lobe ends probably result from hydrodynamical instabilities, perhaps as a result of the high-speed outflow breaking out of the dense AGB envelope. We therefore propose that the overall morphology of Hen 401 is due to the interaction of a bipolar jet, collimated on scales small compared to the nebula (as, e.g., suggested for KJPn8 by Steffen & Lopez 1998), with the progenitor AGB CSE.

The dissipative hydrodynamic interaction of the jet with its surroundings is intermediate between the extreme cases of being fully radiative and fully adiabatic; in the first case (“momentum-driven”), there is no thermal pressure to disperse the shocked material which

builds up a dense plug at the jet-head; in the second (“energy-driven”), hot gas from the jet-head sweeps up the ambient gas into a bubble-like shell structure with a large opening angle (Fig. 1,2, & 3 of MC93). Strong cooling of the shocks at the jet-head is required to produce a significantly narrower shell structure. Using Eqn. 2 of MC93, we can estimate for the case of Hen401 the value of a “cooling” parameter  $\chi_s$ , which is  $<1$  if radiative cooling is important, and  $>1$  if the shock is nearly adiabatic. Taking an AGB mass-loss rate of  $10^{-4} M_{\odot} \text{ yr}^{-1}$  and assuming shock velocities of about  $100 \text{ km s}^{-1}$  (as found in OH231.8 and M1-92) and a jet radius of  $10^{16} \text{ cm}$ , we find  $\chi_s \sim (5 \times 10^{-6} - 0.05)$  for  $r = 10^{16} - 10^{17} \text{ cm}$ . Thus, for reasonable assumptions for the unknown jet radius and shock velocity, we find that the shock is isothermal in most of the Hen401 envelope, resulting in the narrowness of its lobes. Quantitative comparisons of the observed images with such models adapted to the ambient environment provided by an AGB CSE will allow us to constrain the jet physical characteristics (radius/density/velocity/age) and the AGB CSE.

Financial support for this work was provided by NASA through grant GO-06816.01-95A from the Space Telescope Science Institute, operated by the Association of Universities for Research in Astronomy, Inc., under NASA contract NAS5-26555.

## REFERENCES

Aaquist & Kwok 1991, ApJ, 378, 599

Allen, D.A. 1978, MNRAS, 184, 601

Balick, B. 1987, AJ, 94, 671

Balick, B., Alexander, J., Hajian, A.R., Terzian, Y., Perinotto, M., & Patriarchi, P. 1998, AJ, 116, 360

Bobrowsky, M., Zijlstra, A.A., Grebel, E.K., Tinney, C.G., te Lintel Hekkert, P., Van de Steene, G.C., Likkell, L., & Bedding, T.R. 1995, ApJ, 446, L89

Borkowski, K.J., Blondin, J.M., & Harrington, J.P. 1997, ApJ, 482, L97

Bujarrabal, V., Alcolea, J., & Neri, R. 1998, ApJ, 504, 915

Bujarrabal, V., Alcolea, J., Sahai, R., Zamorano, J., & Zijlstra, A.A. 1998, A&A, 331, 361

Bujarrabal, V. & Bachiller, R. 1991, A&A, 242, 247

Hartigan, P., Raymond, J., & Hartmann, L. 1987, ApJ, 316, 323

Herman, J., Burger, J.H., & Penninx, W.H. 1986, A&A, 167, 247

Hrivnak, B.J., Langill, P.P., Su, K.Y.L., Kwok, S. 1999, ApJ, 513, 421

Jura, M. 1986, ApJ, 303, 327

Kwok, S. 1982, ApJ, 258, 280

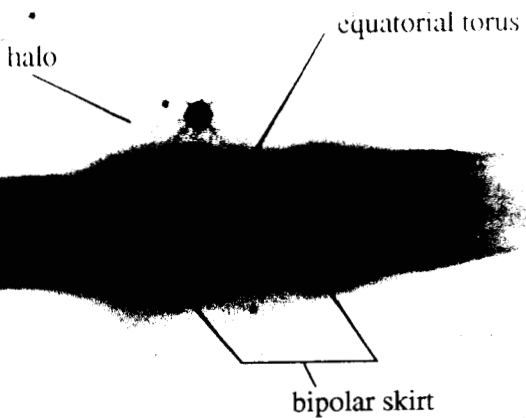
Masson, C.R. & Chernin, L.M. 1993, ApJ, 414, 230 (MC93)

Mellema, G. & Frank, A. 1995, MNRAS, 273, 401

- Mellema, G. 1995, MNRAS, 277, 173
- Pottasch, S.R. 1984, "Planetary Nebulae", Reidel, Dordrecht
- Raga, A.C., Taylor, S.D., Cabrit, S., & Biro, S. 1995, A&A, 296, 833
- Sahai, R., Wootten, A., Schwarz, H.E., & Clegg, R.E.S. 1991, A&A, 251, 560
- Sahai, R., Zijlstra, A., Bujarrabal, V., te Lintel Hekkert, P. 1999a, AJ, 117, 1408
- Sahai, R., te Lintel Hekkert, P., Morris, M., Zijlstra, A., Likkell, L. 1999b, ApJ, 514, L115
- Sahai, R., Ryder, S. et al. 1999c, in preparation
- Sahai, R., et al. 1999d, AJ, in press
- Sahai, R., Hines, D.C., Kastner, J.H., Weintraub, D.A., Trauger, J.T., Rieke, M.J.,  
Thompson, R.I., & Schneider, G. 1998a, ApJ, 492, L163
- Sahai, R., et al., 1998b, ApJ, 493, 301
- Sahai, R. & Trauger, J.T. 1998, AJ, 116, 1357
- Sanduleak, N. & Stephenson, C.B. 1973, ApJ, 185, 899
- Schwarz, H.E., Aspin, C., Corradi, R.L.M., & Reipurth, B. 1997, A&A, 319, 267
- Scarrott, S.M., & Scarrott, R.M.J. 1995, MNRAS, 277, 277
- Schwarz, H.E., Corradi, R.J.M. & Melnick, J. 1992, A&AS, 96, 23
- Steffen, W. & Lopez, J.A. 1998, ApJ, 508, 696
- Truong-Bach, Morris, D., Nguyen-Q-Rieu, & Deguchi, S. 1990, A&A, 230, 431
- Zuckerman, B. & Aller, L. 1986, ApJ 301, 772

Fig. 1.— (a) Wide-band image of the protoplanetary nebula Hen 401 taken with the Planetary Camera (resolution  $0''.0456/\text{pixel}$ ) of WFPC2/HST through the F606W filter. A reverse grey-scale and logarithmic stretch have been used, with the maximum and minimum surface brightnesses on the scale bar shown being  $21 \text{ mJy arcsec}^{-2}$  &  $2.8 \times 10^{-3} \text{ mJy arcsec}^{-2}$ ; (b) A false-color image generated by processing the image in (a) in order to emphasize sharp structures. The processed image,  $I_{m_P} = I_{m_O}/(I_{m_O} + 0.04I_{m_S})$ , where  $I_{m_O}$  is the original image, and  $I_{m_S}$  is obtained by smoothing  $I_{m_O}$ . (c) F656N/F606W and (d) F673N/F606W ratio images of Hen 401. The ratio scale is shown below each of the panels.

F606W



0.01 0.1 1 10 mJy/arcsec<sup>2</sup>

F606W  
(sharp features enhanced)

F656N/F606W

0.1 0.3 0.5

F673N/F606W

0.01 0.03 0.05